Enhanced plasticity of silica glass at high pressure

Daisuke Wakabayashi,[1] Nobumasa Funamori,[1] and Tomoko Sato[2]
[1]*Department of Earth and Planetary Science, University of Tokyo, Tokyo 113-0033, Japan*
[2]*Department of Earth and Planetary Systems Science, Hiroshima University, Higashi-Hiroshima 739-8526, Japan*
(Received 15 May 2014; revised manuscript received 15 December 2014; published 16 January 2015)

We have measured shear flow and residual structural anisotropy of SiO_2 glass uniaxially compressed in a diamond-anvil cell at room temperature with *in situ* optical-microscope and *ex situ* x-ray diffraction techniques, respectively. Large shear flow began at 8−10 GPa and continued at least up to 20 GPa, where the macroscopic differential strain reached 70%. Recovered samples after shear flow were in the fully densified state and showed a large microscopic differential strain of 3% only in the intermediate-range network structure. These phenomena may be attributable to the changes in the Si-O bond covalency and the Si-O-Si bond angle with pressure and stresses.

DOI: 10.1103/PhysRevB.91.014106 PACS number(s): 62.50.−p, 61.43.Fs, 62.20.F−, 91.60.Gf

I. INTRODUCTION

SiO_2 glass is a material of great interest in various research fields, such as condensed-matter physics, materials science, and earth science. It is an archetypal three-dimensional network-forming glass [1] and is categorized as a brittle material because it is a highly covalent solid without long-range order (hence without slip planes seen in crystals). Without long-range order, even metallic glasses are usually not ductile [2]. Although SiO_2 glass (and SiO_2-rich glasses) is a very brittle material, small-scale permanent deformation has long been reported by indentation tests [3,4]. This phenomenon has been explained by the permanent densification [5,6], which is caused by reconstruction of the network structure consisting of SiO_4 tetrahedra (intermediate-range order) [7]. Recent advances in experimental techniques at a very small scale, such as those with an atomic-force microscope and a field-emission-gun scanning electron microscope, have made it possible to conduct detailed *ex situ* observations on the samples recovered from deformation tests [8,9]. These state-of-the-art high-resolution observation techniques have suggested that shear flow, i.e., deformation not attributable to densification, could occur even in SiO_2 glass. However, the observed possible shear flow has been limited to a nanometer scale, and the deformation on a larger scale has been accompanied by cracks [3,4,6,8,9]. Also, molecular-dynamics simulations have predicted that structural anisotropy would remain in the glass after deformation [10]. X-ray diffraction experiments have confirmed the presence of anisotropy in the samples densified by uniaxial compression [11]. However, the information has been limited to the network structure.

In this article, we present the direct evidence of micrometer-scale shear flow (macroscopic strain) and the full information on the residual structural anisotropy (microscopic strain) in SiO_2 glass with *in situ* optical-microscope observations and *ex situ* x-ray diffraction measurements for the samples uniaxially compressed in a diamond-anvil cell. In the case of covalent crystals, samples are expected to fracture without large plastic deformation and not to show any significant residual structural anisotropy by uniaxial compression [11–13]. Our findings contrast sharply with the behavior of covalent crystals and the fact that metallic glasses are less ductile than their crystalline counterparts.

II. EXPERIMENTS

A. Design of experiments

The present study focuses on the deformation behavior of SiO_2 glass at the pressure range below 20 GPa, where the coordination number of silicon remains basically 4. Although it is still somewhat controversial, the pressure-induced structural transformation of SiO_2 glass at room temperature under hydrostatic compression can be summarized as follows [14–16]. (i) SiO_2 glass behaves as a single phase having an ordinary four-coordinated structure below 9 GPa. (ii) Densification in the network structure, i.e., change in intermediate-range order, takes place at pressures between 9 and 13 GPa by rearranging SiO_4 tetrahedra. (iii) SiO_2 glass behaves as a single phase having a fully densified four-coordinated structure at pressures between 13 and 20 GPa. (iv) Change in short-range order takes place at pressures between 20 and 35 GPa by increasing the coordination number of silicon from 4 to 6. (v) SiO_2 glass behaves as a single phase having a six-coordinated structure above 35 GPa. It is known that the change in intermediate-range order remains in a recovered sample after decompression, in contrast to the change in short-range order, which does not remain after decompression.

High-pressure deformation experiments were conducted with a diamond-anvil cell at room temperature. Anvils having a 600-μm flat culet were used with a tungsten-rhenium gasket and an argon pressure medium in three independent runs up to 20 GPa (run 1), 12 GPa (run 2), and 6 GPa (run 3). The three runs were designed so as to clarify the relation between the change in network structure and the deformation behavior of SiO_2 glass (see the preceding paragraph). SiO_2 glass with 99.99% purity in the form of a wire having a diameter of 150 μm was provided by FHP Engineering Limited. Disk-shaped samples were prepared by cutting and polishing the wire to an appropriate thickness to be pinched directly by the two anvils and achieve uniaxial conditions above a designed pressure. The initial thickness was ∼50 μm in runs 1 and 2, and it was ∼75 μm in run 3. A tungsten-rhenium gasket having an initial thickness of 200 μm was preindented to a thickness of ∼90 μm, and then a hole of 250−260 μm in diameter was laser drilled in it to be used as a sample chamber. The sample and small ruby balls (pressure marker) were loaded into the sample

chamber together with cryogenically liquefied argon (pressure medium).

B. *In situ* macroscopic strain measurements

The change in size of the sample was measured by taking optical-microscope images at each pressure through one of the anvils from the direction of the compression axis. Pressure was determined by the ruby-fluorescence method [17]. Strains in the compression axis ε_z and in the radial direction ε_r are defined as follows:

$$\varepsilon_z = \frac{z - z_0}{z_0}, \quad \varepsilon_r = \frac{l - l_0}{l_0}. \tag{1}$$

Here z and l are the lengths in the compression axis and radial direction, respectively. The subscript 0 denotes the values at zero pressure. Assuming uniaxial symmetry, the length change in the compression axis z/z_0 can be calculated by using the following equation, where ρ is the density:

$$\frac{z}{z_0} = \frac{\rho_0}{\rho}\left(\frac{l}{l_0}\right)^{-2}. \tag{2}$$

Therefore, the macroscopic differential strain $\Delta\varepsilon_{\text{macro}}$ is defined by the following equation:

$$\Delta\varepsilon_{\text{macro}} = \varepsilon_r - \varepsilon_z = \frac{l}{l_0} - \left(\frac{\rho_0}{\rho}\right)\left(\frac{l}{l_0}\right)^{-2}. \tag{3}$$

The length change in the radial direction l/l_0 was read from the image at each pressure, and the density change ρ/ρ_0 was assumed to be the same as the literature data [16,18].

C. *Ex situ* microscopic strain measurements

Synchrotron x-ray diffraction measurements on the recovered samples were conducted by using an angle-dispersive method with 50-keV monochromatic x rays and an imaging-plate detector at AR-NE1A of Photon Factory (Tsukuba, Japan). The x-ray diffraction geometry is illustrated in Fig. 1. The largest piece of each recovered sample was glued to the point of a needle and irradiated by x rays from a radial direction (perpendicular to the former compression axis). To calibrate the system, a standard sample (starting material) and a background (without sample) were measured in the same geometry. The exposure time was typically ~10 h for each sample and background.

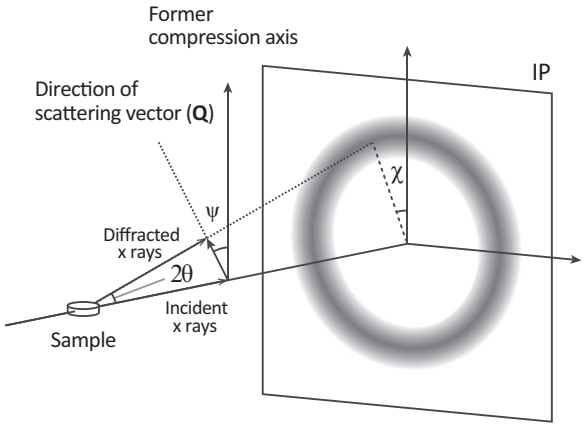

FIG. 1. X-ray diffraction geometry for *ex situ* microscopic strain measurements. There is a relation of $\cos\psi = \cos\chi\cos\theta$.

Assuming uniaxial symmetry, the structure factor $S(Q,\psi)$ can be expanded with spherical harmonics $Y_l^m(\psi)$ (terminated at the second-order term), where ψ is the azimuth angle from the compression axis (Fig. 1), and can be related to the pair distribution function $g(r,\psi)$ as follows [19]:

$$S(Q,\psi) - 1 = S_0^0(Q) + S_2^0(Q)Y_2^0(\psi), \tag{4}$$

$$g(r,\psi) - 1 = g_0^0(r) + g_2^0(r)Y_2^0(\psi), \tag{5}$$

$$g_l^m(r) = \frac{(i)^l}{2n_0\pi^2}\int S_l^m(Q)j_l(Qr)Q^2\,dQ. \tag{6}$$

Here n_0 and j_l are the number density and spherical Bessel function.

The intensity data recorded by a two-dimensional imaging-plate detector were transformed to a two-dimensional structure factor $S(Q,\chi)$ by integrating diffraction intensities within the azimuth angle on the detector χ of $\pm 2.5°$ (Fig. 1) and correcting (or subtracting) background and incoherent scattering intensities. Assuming that the structure factor can be expanded as Eq. (4), $S_0^0(Q)$ and $S_2^0(Q)$ are obtained from $S(Q,\chi)$. $S_0^0(Q)$ and $S_2^0(Q)$ correspond to the average structure (isotropic component) and the uniaxially deviated structure (anisotropic component), respectively. By using Eq. (6), $S_0^0(Q)$ and $S_2^0(Q)$ can be transformed to $g_0^0(r)$ and $g_2^0(r)$, respectively. The analytical procedure to refine the structure factor and pair distribution function was basically the same as described elsewhere [20]; in addition, $S_2^0(Q)$ was assumed to be 0, and $g_2^0(r)$ was assumed to be 0 inside the first peak of $g_0^0(r)$. In all three runs, the refinements were made with the data at $Q < 15\,\text{Å}^{-1}$ and a Fermi-distribution-type termination function.

The first sharp diffraction peak (FSDP) of the structure factor has been considered to be mainly related to the network structure [21,22]. The microscopic differential strain in the network structure (represented by the FSDP) $\Delta\varepsilon_{\text{FSDP}}$ is defined by the following equation [11]:

$$\Delta\varepsilon_{\text{FSDP}} = \frac{Q_{\text{FSDP}}(0°) - Q_{\text{FSDP}}(90°)}{Q_{\text{FSDP}}(54.7°)}. \tag{7}$$

Here $Q_{\text{FSDP}}(\psi)$ is the peak position of the FSDP.

III. RESULTS AND DISCUSSION

A. Deformation of SiO_2 glass under uniaxial compression

The change in size of the sample compressed to 20 GPa in a diamond-anvil cell (run 1) is shown in Fig. 2. The sample was compressed isotropically at low pressures and then compressed uniaxially at high pressures. This figure shows that, after being pinched by the two anvils, the sample deformed largely at a micrometer scale without fracturing at least up to 20 GPa. The pressure dependence of $\Delta\varepsilon_{\text{macro}}$ is shown in Fig. 3. In runs 1 and 2, the samples showed extremely large plastic deformation above 8–10 GPa after the uniaxial condition was achieved at around 6–8 GPa. $\Delta\varepsilon_{\text{macro}}$ reached 70% at 20 GPa. In contrast, in run 3, the sample showed only elastic deformation even after the uniaxial condition was achieved at

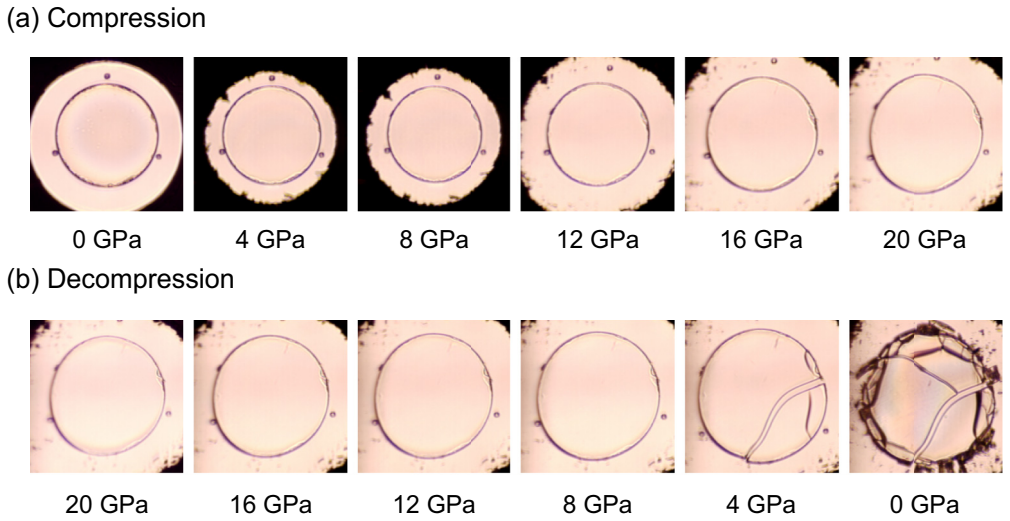

FIG. 2. (Color online) Pressure dependence of the sample size of SiO_2 glass. The optical-microscope images of the disk-shaped sample having an initial diameter of $\sim$150 μm are shown in a sequence of (a) compression and (b) decompression. Ruby balls (three small spheres) and a fraction of gasket (black area) are seen together with the sample. The sample was in air at zero pressure and in an argon pressure medium at the other pressures. The sample size (in the radial direction) first decreased with increasing pressure under isotropic compression and then increased under uniaxial compression. The sample deformed largely without fracturing under uniaxial compression to 20 GPa. Finally, the sample was fractured after the further increase in size on decompression.

around 2–3 GPa. This difference seems to be closely related to the structural transformation of SiO_2 glass, i.e., permanent densification (see Sec. II A). In runs 1 and 2, $\Delta\varepsilon_{\rm macro}$ is about an order of magnitude larger than the microscopic differential strain, e.g., $\Delta\varepsilon_{\rm FSDP} = 0.028$ (as will be shown in Sec. III B),

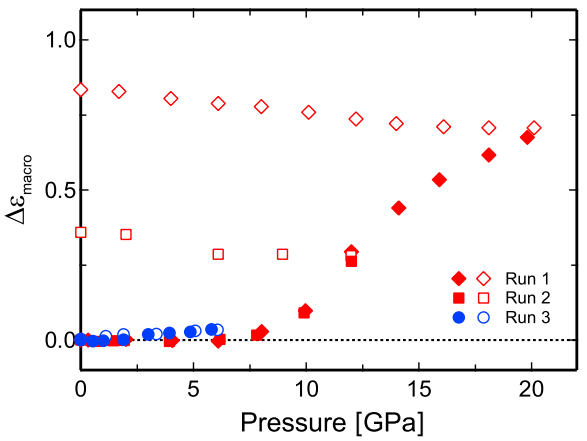

FIG. 3. (Color online) Pressure dependence of the macroscopic differential strain of SiO_2 glass. The solid and open symbols represent the data on compression and decompression, respectively. On compression, the differential strain deviated from zero at around 6–8 GPa in runs 1 and 2 and at around 2–3 GPa in run 3, suggesting that uniaxial conditions were achieved at these pressures. Large plastic deformation was observed in runs 1 and 2 above 8–10 GPa up to 20 GPa, whereas only elastic deformation was observed in run 3 up to 6 GPa. Errors in this plot are very small under hydrostatic conditions. Although errors become somewhat large under nonhydrostatic conditions, they are still small enough to derive the conclusions of the present study (see the text).

providing the conclusive evidence of micrometer-scale shear flow.

To obtain $\Delta\varepsilon_{\rm macro}$, l/l_0 was read from the images. Even if it was read by any means (e.g., measuring a diameter or the distance between scratches on the surface of the sample), the error was negligible within the pressure range of isotropic compression. The deviation from uniaxial symmetry became larger with the progression of shear flow under uniaxial compression (Fig. 2), and the error of $\Delta\varepsilon_{\rm macro}$ due to the reading became as large as $\pm$0.025 at 20 GPa. The error got even larger after the fracture of the sample on decompression. ρ/ρ_0 was assumed to be the same as the literature data [16,18]. However, the occurrence of shear flow may have affected the structural transformation and thus the density as a function of pressure (see Sec. III C). This could be an additional error source. Moreover, under uniaxial compression, the pressure measured with ruby balls corresponds to confining pressure, and the difference between the hydrostatic component of stress tensor and the confining pressure could be as large as 2 GPa at 20 GPa, estimated from the literature data [11,23]. Nevertheless, because $\Delta\varepsilon_{\rm macro}$ is quite large (on compression above 8–10 GPa and subsequent decompression), these errors do not affect the conclusion of the preceding paragraph.

In runs 1 and 2, the samples were fractured when decompressed down to around 4–6 GPa. On decompression, shear flow becomes less likely to occur (see Sec. III C), and the confining pressure in the radial direction becomes small. Therefore, the fracture of the sample may be due to the increase in differential stress and the decrease in fracture strength.

B. Residual structural anisotropy in deformed SiO_2 glass

The structure factor $S(Q,\psi)$ and pair distribution function $g(r,\psi)$ of the sample recovered from 20 GPa (run 1) are shown

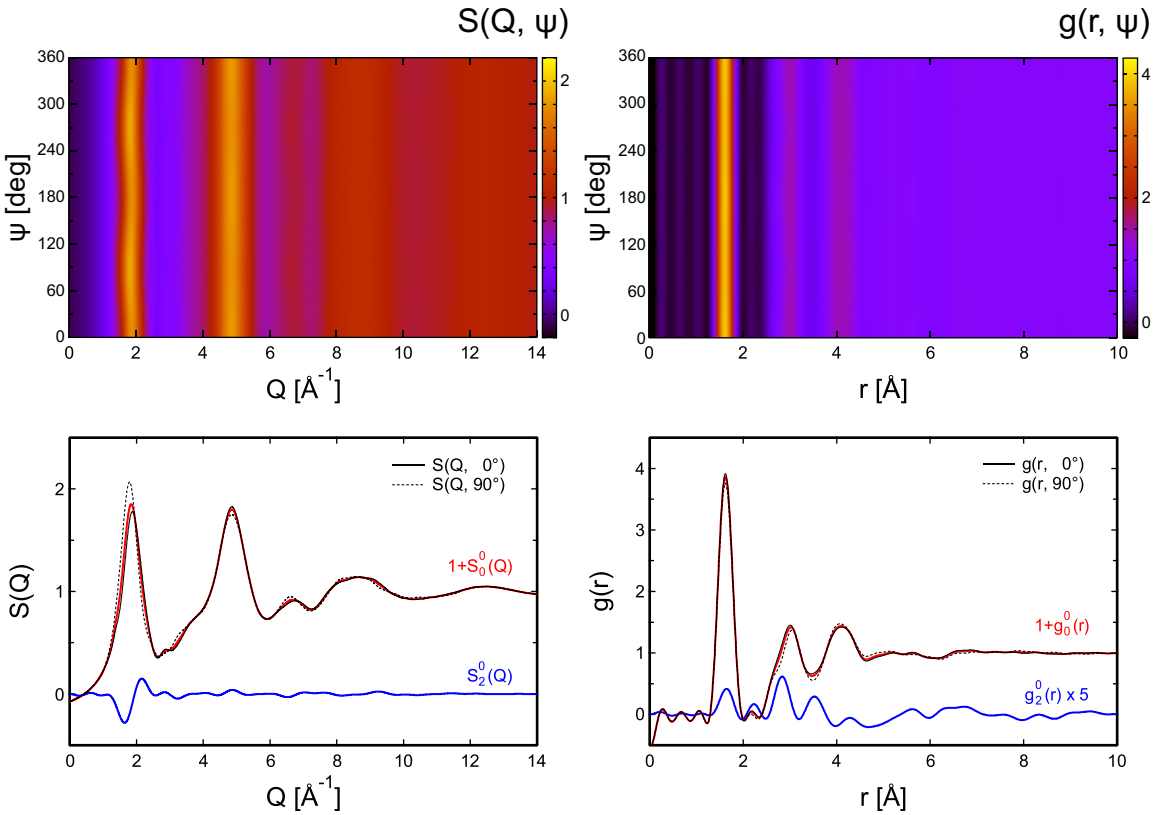

FIG. 4. (Color online) Structure factor $S(Q,\psi)$ and pair distribution function $g(r,\psi)$ of plastically deformed SiO_2 glass. The upper column shows the azimuthal dependence of the structure factor and pair distribution function. The black solid and dotted lines in the lower column represent the structure factor and pair distribution function in the former compression axis and radial direction, respectively. The position of the first sharp diffraction peak of the structure factor shows significant anisotropy. This peak is considered to be associated with the network structure consisting of SiO_4 tetrahedra, and therefore the anisotropy indicates that a large differential strain, as much as ~3%, remained in the network structure of the recovered sample. On the other hand, the structure factor at a higher-Q range does not show any significant anisotropy as seen in the first peak, indicating that a differential strain did not remain in the basic structural unit of the SiO_4 tetrahedron.

in Fig. 4. A significant azimuthal dependence of the position of the FSDP suggests that a large differential strain $\Delta\varepsilon_{\mathrm{FSDP}}$ as much as 0.028 remained in the network structure. On the other hand, the structure factor does not show any significant azimuthal dependence at a higher-Q range. In the pair distribution function, a relatively large anisotropy is seen only above ~3 Å, corresponding to the Si-Si distance in the network structure, whereas no obvious anisotropy is seen in the first peak, corresponding to the Si-O bond of the SiO_4 tetrahedron. The mean peak position of the FSDP [strictly, $Q_{\mathrm{FSDP}}(54.7^\circ)$ or the peak position in $1+S_0^0(Q)$], 1.845 $\mathrm{Å}^{-1}$, suggests that the recovered sample was in the fully densified state (~20% increase in density); the position of the FSDP is a good measure of density [16]. The intensity of the FSDP shows a slight azimuthal dependence, suggesting that the network structure might be less ordered along the compression axis. The result of the recovered sample in run 2 was identical to that in run 1, whereas that in run 3 was identical to the result of the starting material. These results reveal that a very large differential strain can remain only in the network structure of the plastically deformed sample. Therefore, the occurrence of shear flow seems to be strongly related to reconstruction of the network structure.

C. Mechanism of deformation and densification

The onset-pressure condition of plastic deformation is close to that of permanent densification as discussed in Sec. III A. Moreover, a large differential strain can remain only in the network structure of the plastically deformed sample as discussed in Sec. III B. These observations strongly suggest that plastic deformation and permanent densification may originate from the same mechanism, i.e., reconstruction of the network structure. Upon decompression, ~20% permanent densification and ~3% residual differential strain in the network structure were quenched in both the samples from 12 and 20 GPa; $Q_{\mathrm{FSDP}}(54.7^\circ) = 1.845\ \mathrm{Å}^{-1}$, $\Delta\varepsilon_{\mathrm{FSDP}} = 0.028$ in run 1 and $Q_{\mathrm{FSDP}}(54.7^\circ) = 1.841\ \mathrm{Å}^{-1}$, $\Delta\varepsilon_{\mathrm{FSDP}} = 0.027$ in run 2. The sample from 60 GPa in our preliminary work [11] showed similar values to those in runs 1 and 2, although it could be in a different state because it had once transformed to a six-coordinated state and then recovered as a densified glass (see Sec. II A) and its structural information could not be fully measured [11]. In any case, it seems that the pressure and stresses applied on SiO_2 glass are relaxed (to be in more stable states) by phase transformation and shear flow through reconstruction of the network structure and that they cause the permanent densification up to 20% and

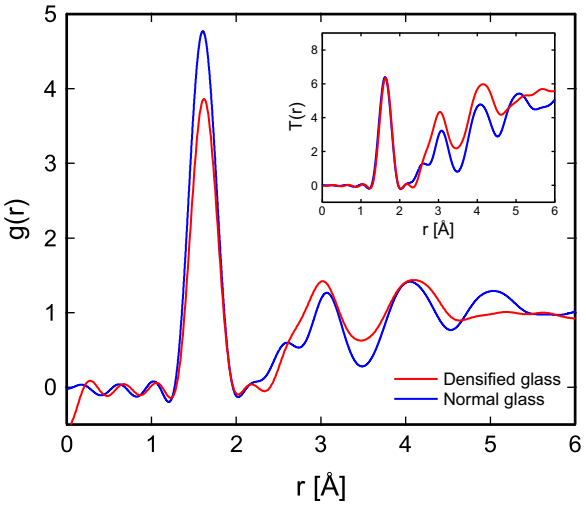

FIG. 5. (Color online) Pair distribution function of densified and normal SiO_2 glasses. The term $1 + g_0^0(r)$, which is independent of the azimuth angle, of the sample in the fully densified state after plastic deformation (the same as shown in Fig. 4) is compared with that of the starting material. The Si-O bond length, corresponding to the first peak, is longer in densified glass than in normal glass, suggesting the weakening of the bond in densified glass. Also, the Si-Si distance, corresponding to the peak at ∼3 Å, is shorter in densified glass, suggesting the decrease in the Si-O-Si bond angle. The difference in height of the first peak is due to the difference not in coordination number but in number density [Eq. (6)]. The total correlation function $T(r)$, defined as $4\pi n_0 r g(r)$, is shown in the inset to demonstrate that the coordination numbers of the two glasses are almost the same.

permanent differential strain in the network structure up to 3%. The permanent densification has been considered to take place at a narrow pressure interval between 9 and 13 GPa under hydrostatic conditions and begin at lower pressures and end at higher pressures with nonhydrostatic stresses [16]. In our experiments, however, the permanent densification was already completed in the recovered sample from 12 GPa despite the uniaxial compression. The unique feature of our experiments is the occurrence of large shear flow. Large-scale shear flow is accompanied by considerable reconstruction of the network structure and therefore supposed to facilitate the permanent densification. This picture is consistent with the model in which the yield criterion of SiO_2 glass is expressed as a function of two variables, pressure and von Mises stress [9,24].

The comparison of structures between densified and normal glasses is shown in Fig. 5. The Si-O bond length of densified glass, 1.634 Å, is longer than that of normal glass, 1.621 Å, suggesting that this bond becomes less covalent. The weakening of the bond is supposed to make large-scale shear flow possible (Fig. 2). In fact, nanometer-scale indentation tests have suggested that shear flow occurs relatively easily in glasses with weaker bonds; shear flow would occur less difficultly in densified glass than in normal glass [8]. Also, the strength of densified glass at 10–20 GPa has been reported to be about half that of normal glass at zero pressure [11,23]. This seems consistent with the fact that shear flow occurs more easily in densified glass. The oxygen K-edge x-ray Raman spectroscopy has suggested that the change in electronic states may occur at the similar pressure range [25]. This could also be related to the change in deformation behavior, although the argument of the change in electronic states is still controversial [25–27].

The Si-Si distance of densified glass is shorter than that of normal glass (see the peak at ∼3 Å in Fig. 5), suggesting the decrease in the Si-O-Si bond angle. In the pressure range of our experiments, it is expected that the basic structural unit (short-range order) does not change from the SiO_4 tetrahedron to the SiO_6 octahedron and therefore the coordination number does not increase significantly (see Sec. II A). Indeed, the coordination number calculated from $g(r)$ shown in Fig. 5 is 3.8 for densified glass (cf. 3.9 for normal glass). The ^{29}Si NMR spectroscopy has also suggested that the amount of five- and six-coordinated states in densified glass is below the detection limit ($< 0.3\%$) [28]. On the other hand, molecular-dynamics simulations have suggested the presence of a significant amount of five- and six-coordinated states in densified glass (up to 20%) [29]. In any case, the decrease in the Si-O-Si bond angle is supposed to facilitate the rearrangement of the network through five- and/or six-coordinated transient states [29–31]. The decrease in the Si-O-Si bond angle is closely related to the weakening of the Si-O bond discussed in the preceding paragraph. On decompression, the Si-O-Si bond angle increases, and the rearrangement becomes less likely to occur with decreasing pressure. This may cause the fracture of the sample (Fig. 2) and may also leave the permanent densification and permanent differential strain. This picture is consistent with the model in which a modified network structure is quenched to zero pressure due to the kinetic barrier [32].

IV. SUMMARY

It has been clarified that applying high pressure and high stresses on SiO_2 glass facilitates the weakening of the Si-O bond and resultant reconstruction of the network structure and then causes the phase transformation accompanied by the permanent densification up to 20% and the shear flow accompanied by the permanent differential strain in the network structure up to 3%. The decrease in the Si-O-Si bond angle is a key to facilitate the rearrangement of the network probably through five- and/or six-coordinated transient states.

ACKNOWLEDGMENTS

The authors thank T. Kikegawa, K. Watanabe, and H. Yamauchi for experimental support. Synchrotron x-ray diffraction experiments were carried out at Photon Factory. D.W. is supported by Research Fellowships of the Japan Society for the Promotion of Science for Young Scientists. This work was, in part, supported by a Grant-in-Aid for Scientific Research (Japan) and Special Coordination Funds for Promoting Science and Technology (Japan).

[1] W. H. Zachariasen, J. Am. Chem. Soc. **54**, 3841 (1932).
[2] C. A. Pampillo, J. Mater. Sci. **10**, 1194 (1975).
[3] E. W. Taylor, Nature (London) **163**, 323 (1949).
[4] D. M. Marsh, Proc. R. Soc. London, Ser. A **279**, 420 (1964).
[5] P. W. Bridgman and I. Šimon, J. Appl. Phys. **24**, 405 (1953).
[6] F. M. Ernsberger, J. Am. Ceram. Soc. **51**, 545 (1968).
[7] S. Susman, K. J. Volin, D. L. Price, M. Grimsditch, J. P. Rino, R. K. Kalia, P. Vashishta, G. Gwanmesia, Y. Wang, and R. C. Liebermann, Phys. Rev. B **43**, 1194 (1991).
[8] T. Rouxel, H. Ji, J. P. Guin, F. Augereau, and B. Rufflé, J. Appl. Phys. **107**, 094903 (2010).
[9] R. Lacroix, G. Kermouche, J. Teisseire, and E. Barthel, Acta Mater. **60**, 5555 (2012).
[10] C. L. Rountree, D. Vandembroucq, M. Talamali, E. Bouchaud, and S. Roux, Phys. Rev. Lett. **102**, 195501 (2009).
[11] T. Sato, N. Funamori, and T. Yagi, J. Appl. Phys. **114**, 103509 (2013).
[12] J. M. Christie, H. C. Heard, and P. N. LaMori, Am. J. Sci. **262**, 26 (1964).
[13] L. Marques, M. Mezouar, J.-L. Hodeau, M. Núñez-Regueiro, N. R. Serebryanaya, V. A. Ivdenko, V. D. Blank, and G. A. Dubitsky, Science **283**, 1720 (1999).
[14] T. Sato and N. Funamori, Phys. Rev. Lett. **101**, 255502 (2008).
[15] T. Sato and N. Funamori, Phys. Rev. B **82**, 184102 (2010).
[16] D. Wakabayashi, N. Funamori, T. Sato, and T. Taniguchi, Phys. Rev. B **84**, 144103 (2011).
[17] H. K. Mao, J. Xu, and P. M. Bell, J. Geophys. Res.: Solid Earth **91**, 4673 (1986).
[18] T. Sato, N. Funamori, and T. Yagi, Nat. Commun. **2**, 345 (2011).
[19] Y. Suzuki, J. Haimovich, and T. Egami, Phys. Rev. B **35**, 2162 (1987).
[20] T. Sato, N. Funamori, and T. Kikegawa, Rev. Sci. Instrum. **81**, 043906 (2010).
[21] S. R. Elliott, Nature (London) **354**, 445 (1991).
[22] Q. Mei, C. J. Benmore, S. Sen, R. Sharma, and J. L. Yarger, Phys. Rev. B **78**, 144204 (2008).
[23] C. Meade and R. Jeanloz, Science **241**, 1072 (1988).
[24] G. Kermouche, E. Barthel, D. Vandembroucq, and Ph. Dubujet, Acta Mater. **56**, 3222 (2008).
[25] J.-F. Lin, H. Fukui, D. Prendergast, T. Okuchi, Y. Q. Cai, N. Hiraoka, C.-S. Yoo, A. Trave, P. Eng, M. Y. Hu, and P. Chow, Phys. Rev. B **75**, 012201 (2007).
[26] M. Wu, Y. Liang, J.-Z. Jiang, and J. S. Tse, Sci. Rep. **2**, 398 (2012).
[27] N. Li, R. Sakidja, S. Aryal, and W.-Y. Ching, Phys. Chem. Chem. Phys. **16**, 1500 (2014).
[28] X. Xue, J. F. Stebbins, M. Kanzaki, P. F. McMillan, and B. Poe, Am. Mineral. **76**, 8 (1991).
[29] F. Yuan and L. Huang, Sci. Rep. **4**, 5035 (2014).
[30] E. M. Stolper and T. J. Ahrens, Geophys. Res. Lett. **14**, 1231 (1987).
[31] S. Tsuneyuki and Y. Matsui, Phys. Rev. Lett. **74**, 3197 (1995).
[32] F. S. El'kin, V. V. Brazhkin, L. G. Khvostantsev, O. B. Tsiok, and A. G. Lyapin, JETP Lett. **75**, 342 (2002).